Int J Adv Manuf Technol (2016) 87:2337–2352
DOI 10.1007/s00170-016-8636-y

ORIGINAL ARTICLE

Experimental studies on optimized mechanical properties while dissimilar joining AA6061 and AA5010 in a friction stir welding process

Masoud Ahmadnia[1] · **Saeid Shahraki**[2] · **Mojtaba Ahmadi Kamarposhti**[3]

Received: 30 October 2015 / Accepted: 17 March 2016 / Published online: 28 March 2016

Abstract One of the advantages of friction stir welding process is its ability to join dissimilar metals and alloys. The aim of this work is to predict mechanical properties, i.e., tensile strength, hardness, and elongation of aluminum 6061 to aluminum 5010 joint that is fabricated by friction stir welding process. Here, response surface methodology based on central composite design with three parameters, five levels, and 20 runs was used to conduct experiments and to develop mathematical regression models. The three welding parameters considered were tool rotary speed, welding speed, and plunging depth. Analysis of variance was then performed to check the adequacy of developed models. The effects of process factors on mechanical properties were studied using developed mathematical models and on the basis of macrostructure and microstructure characterization and fractography of joints which are examined by optical and scanning electron microscopy. Finally, optimal parameter setting was identified by performing optimization through desirability approach function.

Keywords Friction stir welding · Dissimilar aluminum alloys · Response surface methodology · Microstructure characterization · Fractography · Optimization

✉ Mojtaba Ahmadi Kamarposhti
mj.ahmadi5925@outlook.com

[1] Department of Mechanical Engineering, Khajenasir University of Technology, Tehran, Iran

[2] Department of Mechanical Engineering, University of Zabol, Zabol, Iran

[3] Department of Mechanical Engineering, Sari Branch, Islamic Azad University, Sari, Iran

1 Introduction

Fusion welding of dissimilar aluminum alloys is very challenging mainly due to the formation of low melting eutectics by the constituent elements resulting in weld solidification cracking (hot cracking) [1]. Solidification cracking in aluminum alloys is extremely sensitive to weld metal composition, which depends on the composition of the filler metal, composition of the base metal, and amount of dilution. Therefore, one must carefully choose the filler composition and/or welding parameters such that the resultant weld composition is not susceptible to solidification cracking [1]. Solid-state welding processes are ideally suited for welding of dissimilar aluminum alloys. Because these processes do not involve melting, the issue of weld solidification cracking does not arise. Similarly, solid-state welding processes overcome a variety of other problems in fusion welding of aluminum alloys such as porosity, segregation, brittle intermetallic formation, and heat-affected zone liquation cracking [1]. Among the solid-state welding processes, friction stir welding is very attractive for welding of dissimilar aluminum alloys as it is suitable for producing welds in a variety of joint configurations, including butt joints. Figure 1 demonstrates a schematic view of friction stir welding (FSW) process along with its influential parameters.

Aluminum series 6xxx and 5xxx are two industrial alloys with high strength and good formability, respectively, which are extensively used in automobile, aerospace, marine, and transportation industries. Both series are subjected to be friction stir welded separately by various researches. For instance, Elengovan et al. [2] analyzed the effect of tool pin profile and other FSW parameters on tensile strength of friction stir welded AA6061 through construction of a mathematical model. As a result, the joints fabricated by square pin profile have superior tensile strength due to appropriate material flow and

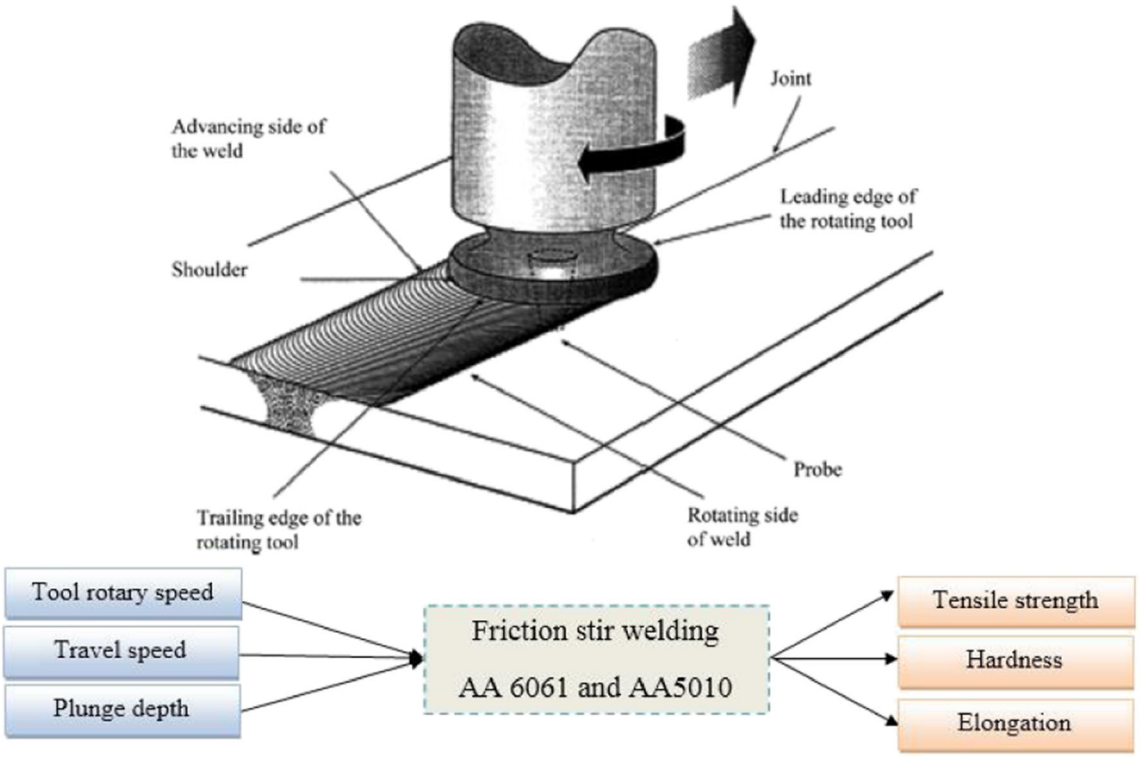

Fig. 1 A schematic view of FSW process along with influential parameters

better plasticization. Rajakumar et al. [3] conducted an extensive range of experiments to study the effects of tool geometry and FSW main parameters on tensile strength, hardness, and corrosion rate of AA6061 FSWed joints. They showed that tool rotary speed and tool shoulder diameter are the most significant factors having great influence on mechanical properties and corrosion rate. Lee at al. [4] showed that the friction stir welding parameters significantly affect the microstructure of the welded zone and, subsequently, these variations highly influence the mechanical properties. Ramalu et al. [5] analyzed the effects of tool rotary speed, welding speed, plunge depth, and tool shoulder diameter on the formation of voids in the friction stir processed (FSP) zone. They showed that the higher the value of rotational speed, the lower the travel speed and the higher the plunge depth, causing a higher heat input in the FSP zone and removing defects such as tunnel and pin hole. Similarly, for aluminum alloy series 5xxx, there are various papers. Kwon et al. [6] used the FSW process to fabricate joints from 5052 alloy and analyze the effect of rotational speed of tool on tensile strength. They showed that by an increase in tool rotary speed, the tensile strength approaches to that of the base metal, but no significant improvement in elongation is observed. Han et al. [7] analyzed the effects of tool rotary speed and welding speed on mechanical properties of the AA5083 joint. They showed that low welding speed and low tool rotary speed yield higher joint strength and elongation ratio. Moshwan et al. [8] studied the effects of welding speed on mechanical properties, force generation, and microstructure of AA5052 joints. They showed that rotational speed of 1000 RPM causes high joint efficiency, hardness, and fine grain structure.

There are limited number of works regarding dissimilar joining of AA 5xxx series to AA 6xxx series. In this case, Jamshidi-Aval et al. [9] studied the effect of welding arrangement and process parameters in friction stir welding of AA5086-O and AA6061-T6. The mechanical properties of the welded samples are investigated by a three-dimensional model. Alvarez et al. [10] carried out dissimilar FSW experiments with a right-hand threaded cylindrical pin on 6082-T6 and 5754-H111 aluminum sheets. Palanivel et al. [11] performed a series of experiments to analyze the effect of tool rotational speed and pin profile on the microstructure and tensile strength of dissimilar friction stir welded AA5083-H111 and AA6351-T6 aluminum alloys. Leitao et al. [12] studied FSW experiments on both AA5083 and AA6082 aluminum alloys. Their main purpose was to analyze the influence of high-temperature plastic behavior of the two alloys on the friction stir weldability. The results indicate that compared to the mechanical characterization results of the base material, the AA6082 alloy displays good weldability with FSW due to the sensitivity to intense flow softening during the high-temperature plastic deformation. Kasman [13] performed an experimental study to identify optimum FSW parameter setting. They combined Taguchi method with grey relational

analysis and found that the ratio of shoulder diameter to pin diameter, followed by welding speed and tool rotary speed, has great impact on overall welding quality.

When dissimilar alloys are subjected to be welded by the FSW process, prediction of the amount of heat generation, material flow, and mechanical properties of the joints by means of theoretical analysis is difficult. Therefore, numerical analysis and data mining approaches based on experimental observations can serve as practical tools for predicting the aforementioned phenomena. In the case of numerical simulation of FSW process, Zhang et al. [14–19] developed valuable models for predicting heat generation, type of contact, grain growth, and temperature history during FSW of series 6xxx and 2xxx aluminum alloys. However, in the case of dissimilar joining, there are a few number of works. Jamshidi Aval et al. [20] performed an experimental and numerical study to simulate thermomechanical responses of material during dissimilar joining of AA5086 and AA6061. They attempted to predict thermal history and residual stress during the process and compared them with experimental observation. The obtained results were in reasonable agreement with experimental approaches. Al-Badour et al. [21] developed a 3D FEM model based on the Coupled Eulerian-Lagrangian method to simulate the friction stir welding of dissimilar Al6061-T6 and Al5083-O aluminum alloys using different tool pin profiles. The model was further validated using measured temperatures. The finite element results show that maximum temperatures at the weld joint were below the materials' melting point. Placing the harder alloy (Al6061-T6) at the advancing side led to a decrease in maximum process temperature and strain rate, but increased the tool reaction loads. Kishore et al. [22] developed a two-dimensional steady-state model for friction stir welding of two dissimilar joints, i.e., AA6061-AA5083 and AA2024-AA7075. The temperature distribution and material flow around the tool are studied for the different position of materials, process parameters, and tool profiles. It is seen that the peak temperature is generated on the harder material side with a change in position of materials. The trivex pin profile is found to be better than the circular pin profile by reducing the welding traverse force and an efficient symmetric mixing of materials. Although numerical approaches are applicable tools for predicting the behavior of the FSW process like material flow, applied load, strain, temperature, and residual stress, several simplifications and assumptions should be performed for deriving the simulation. Furthermore, obtaining final mechanical properties such as tensile strength, hardness, and elongation is difficult when numerical approaches are utilized. To overcome the problem, data mining approaches based on experimental design is proposed by various researchers for simultaneous prediction and optimization of the FSW process achieving desirable mechanical properties. In this case, Padmanban et al. [23] combined simulated annealing with response surface methodology to find an optimal setting of tool rotary speed and travel speed for maximization of tensile strength of AA7075-AA2024 dissimilar joints. They showed that 1086 RPM tool rotary speed and 14.7 travel speed cause the higher value of tensile strength. Elastharasan et al. [24] applied response surface methodology (RSM) for predicting tensile strength, yield strength, and displacement of dissimilar joints AA6061-AA7075. They further analyzed the parametric influence of factors. Gupta et al. [25] used a hybrid approach comprising grey relational analysis to optimize processing factors in dissimilar joining of AA6063-AA5083. The optimal set of process parameters using the hybrid approach was found as 900 r/min of tool rotational speed, 60 mm/min of welding speed, 18 mm of shoulder diameter, and 5 mm of pin diameter. Palanivel et al. [26] used RSM for predicting and optimizing the tensile strength of dissimilar aluminum alloy (AA6351 T6-AA5083 H111). They showed that using the straight square pin profiled tool with tool rotational speed of 950 r/min, welding speed of 63 mm/min, and 14.7 kN causes a maximum value of tensile strength.

According to the above literate survey, friction stir welding of AA6061-T6 to AA 5010 has not been reported so far. Also, there is not seen a paper regarding multi-objective optimization of friction stir welding process taking into account different processing factors as well as various responses. Also, microstructural analysis and material characterization of joints fabricated at optimal level were not analyzed. Hence, this article deals with statistical design of experiment and application of RSM in developing empirical relationships relating important input variables, tool rotary speed, welding traverse speed, and plunge depth to the tensile strength, hardness, and elongation of dissimilar joints. Further, this article illustrates how a number of overlapping response surfaces can be used to select the operating conditions necessary to achieve the desired specifications and for the optimization of the friction stir welding of AA5010 and AA6061. It should be emphasized that the range selected for parameters, the results, and the conclusions refer specifically to the macrostructure and microstructure, the fractography, and XRD analysis of the weld region.

2 Experiments

2.1 Experimental equipment and materials

In order to study the effects of FSW process parameters on mechanical properties of friction stir welding of dissimilar aluminum alloys (e.g., AA6061 and AA5010), the rolled plates of 3 mm thickness were cut into the required sizes (100 mm × 150 mm) by power hacksaw cutting and milling. Then, a clamping system was designed and mounted on a Tabriz/4301 (15 hp, 3000 RPM) milling machine modified with FSW tool attachment to secure the plates in their proper

Table 1 Chemical composition of AA6061 and AA5010 (all the values are in percent)

Type	Al	Ti	Zn	Mn	Cr	Cu	Fe	Si	Mg
AA6061	Bal	0.02	0.02	0.06	0.17	0.28	0.33	0.62	0.9
AA5010	Bal	0.1	0.3	0.2	0.15	0.25	0.7	0.4	0.4

positions. Non-consumable tools with various pin profile, made of high carbon steel, were used to fabricate the joints. The chemical compositions and mechanical properties of base metals are presented in Tables 1 and 2, respectively. Figure 2 indicates schematic and actual views of tools with their various pin profiles.

The specimens for metallographic examination were sectioned to the required sizes from the joint comprising the FSP zone and then polished using different grades of emery papers. Final polishing was done using the diamond compound (1 μm particle size) in the disc polishing machine. The polished samples were etched using 10 % NaOH to show general flow structure of the alloy. Macrostructural and microstructural analyses have been carried out using a light optical microscope (VERSAMET-3) incorporated with an image analyzing software (Clemex Vision).

In order to measure the ultimate tensile strength and elongation of welded samples, the tensile test specimens which cut from the welded joint have been gripped by grippers of a 100-kN servo-controlled universal testing machine and the values of tensile strength and elongation are measured. Also, to measure the microhardness of the welded zone, the Vickers's microhardness testing machine (Shimadzu, model HMV-2T) with 0.05 kg load at 15 s is employed.

2.2 Experiments procedures

In the present study, the experiments are divided into two main stages. The first stage of experiments is designed to find the appropriate tool pin profile to reach the highest tensile strength, hardness, and elongation. Here, nine experiments were conducted with three types of pin profiles (e.g., straight cylindrical, triangular, and square types) and under different heat generation conditions (e.g., low heat, middle heat, and high heat). Here, the reason for the selection of various heat inputs is to show replicability of the results. This is because the heat generation is varied by a variation of processing parameters. According to Arora et al. [27], stir zone geometry is changed under different conditions. Further, according to Zhang et al. [14], the heat input differs in low and high angular velocity. In addition, Zhang and Chem [15] also reported that the strain hardening coefficient and the plastic strain are also varied by change in FSW/FSP parameters. Hence, to show the rigidity of the results, various conditions should be tested. Hence, to select the best pin profile, various conditions should be considered and the results should have repeatability.

Table 2 Mechanical properties of AA6061 and AA5010

Type	Yield strength (MPa)	Tensile strength (MPa)	Elongation (%)	Hardness (Vickers)
AA6061	302	334	12.24	105
AA5010	211	264	41	82

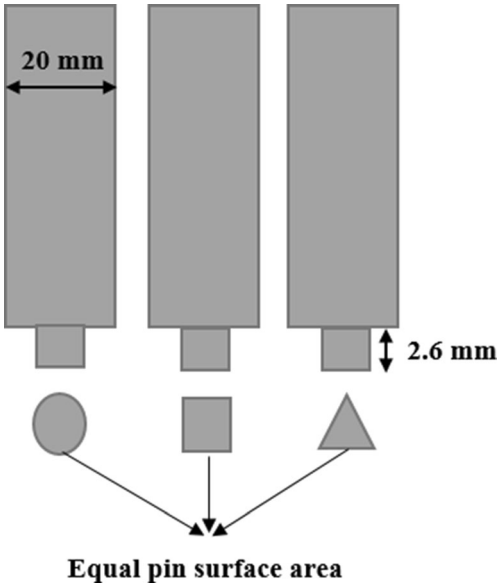

Fig. 2 A schematic drawing of FSW tools with different pin profiles

According to Zhang et al. [16], heat generation in interface of tool and sheet comprised three sources: heat generation from the shoulder face, i.e., W_1, heat generation from the pin side, i.e., W_2, and heat generation from the pin face, i.e., W_3. The following presents dependency of heat generation to processing parameters.

$$W_1 = \frac{3}{2}\pi\omega\mu P\left(R^3{}_{shoulder} - R^3{}_{pin}\right) \quad (1)$$

$$W_2 = 2\pi\omega\mu P R^2{}_{pin} H_{pin} \quad (2)$$

$$W3 = \frac{2}{3}\pi\omega\mu P R^3{}_{pin} \quad (3)$$

where ω is the tool rotary speed, μ is the friction coefficient, P is the pressure applied by a plunging action, $R_{Shoulder}$ is the shoulder diameter, R_{Pin} is the pin diameter, and H_{Pin} is the pin length.

Zhang et al. [14] also mentioned that the heat flux density in the interface was significantly affected by frictional stress (i.e., applied pressure) and slipping rate (Eq. 4). Also, the

Table 3 Different heat generation conditions for conducting first stage of experiments

Heat generation condition	Tool rotary speed (RPM)	Welding speed (mm/min)	Plunging depth (mm)
High heat	1200	40	0.4
Middle Heat	800	60	0.2
Low heat	400	80	0.1

slipping rate can be determined by a velocity difference between welding tool and workpiece (Eq. 5).

$$q = P\gamma \tag{4}$$

$$\gamma = \delta(R\omega - V_0) \tag{5}$$

where q is heat flux density, γ is the slipping rate, δ is the slipping factor, and V_0 is the travel speed.

Therefore, according to the following equations, it is inferred that the higher values of tool rotational speed cause higher heat generation. On the other hand, higher values of applied pressure, i.e., P, cause higher heat generation. It can be noted that the applied pressure is significantly affected by a plunging action of the tool. Therefore, the higher value of plunge depth causes higher pressure and subsequently results in higher heat generation. In addition, a higher value of travel speed, i.e., V_0, causes reduction in heat flux density and corresponding generation and opposite. Thus, it is inferred that from the aforementioned equations, in a low heat generation condition, the tool rotary speed and plunge depth are low and the welding travel speed is high. In opposite, in a high heat generation condition, the tool rotary speed and plunge depth are high and the welding travel speed is low. However, in the middle condition, all the three parameters were chosen at their moderate levels. Variation of the aforementioned conditions significantly affects formation of microstructure, macrostructure, and weld morphology that determine weld properties.

The experiments at the first stage were carried out to show the repeatability of the results under different processing parameters regarding selection of best pin profile. Table 3 displays the values of processing parameters for various heat generation conditions which are defined for tool pin profile design. Also, Table 4 presents the experiments at the first stage along with measured values of tensile strength, hardness, and elongation. In this stage, the pin profile that causes higher tensile strength, hardness, and elongation is used for conducting a second stage of experiments.

The second stage of experiments is designed based on central composite design (CCD) of experiments to study effects of the FSW process predominant factors such as tool rotary speed, welding speed, and plunge depth on mentioned mechanical properties. Table 5 indicates the factors of the second stage of experiments along with their levels according to CCD. Here, 20 experiments have been designed to form a design matrix. Table 6 presents the experiments of the second stage of experiments along with obtained values of tensile strength, hardness, and elongation.

3 Results

3.1 Finding appropriate pin profile

As explained, the aim of the first stage of experiments is to find an optimum tool pin profile considering higher tensile strength, hardness, and elongation. The results of the first stage of experiments for cylindrical, triangular, and square tool pin profiles are presented in Fig. 3. From the figure, it is seen that irrespective to frictional condition, tools with a square type pin profile yield maximal mechanical properties. Next to the square profile, the triangular pin profile results in higher tensile strength, hardness, and elongation when compared to the straight cylindrical profile. During the friction stir welding process, the type of pin profile directly affects material flow and shearing action of plasticized materials. In the next section (i.e., Sect. 4), a discussion about how tool pin

Table 4 Experiments of first stage along with measured values of TS, HV and EL

No	Tool pin profile	Heat Generation	Tensile strength (MPa)	Hardness (HV)	Elongation (%)
1	Cylindrical	Low heat (Table 3)	132	57	6.4
2	Cylindrical	Medium heat (Table 3)	173	95	8.9
3	Cylindrical	High heat (Table 3)	151	75	12.1
4	Triangular	Low	135	72	8.6
5	Triangular	Medium	175	106	14.1
6	Triangular	High	157	88	17.2
7	Square	Low	156	84	15.3
8	Square	Medium	197	129	19.5
9	Square	High	176	105	24

Table 5 Factors of second stage of experiments along with their levels based on CCD

Parameters	Coded values at different levels				
	−1.68	−1	0	1	1.68
Tool rotary speed (RPM)	460	600	800	1000	1140
Welding speed (mm/min)	24	40	60	80	97
Plunging depth (mm)	0.03	0.1	0.2	0.3	0.37

profile affects material flow and microstructural evolution will be presented by the use of macrographical images and microstructure of weld nugget. According to the results, for the next stage of experiment, the square pin profile is used to fabricate the joints due to its higher mechanical properties.

3.2 Development response surface models of mechanical properties

To find the response of process factors with respect to process quality characteristics, second-order mathematical models of tensile strength, hardness, and elongation were developed through regression analysis. To develop these models, a commercial statistical package Design-Expert V7 was utilized and the validity of full quadratic models were evaluated by analysis of variance (ANOVA) and coefficient of determination, i.e., R^2. The second-order mathematical models of responses including linear, quadratic, and interaction terms of factors are given in Eqs. 1, 2, and 3.

$$TS = 255.55 + 0.592N + 4.17f + 555.54d - 3.51 \times 10^{-4}N^2 - 0.03f^2 - 824.18d^2 - 3.12 \times 10^{-4}Nf - 0.15Nd - 1.37fd \quad (6)$$

$$HV = -311 + 0.61N + 4.32f + 551.6d - 3.63 \times 10^{-4}N^2 - 0.031f^2 - 869.2d^2 - 3.75 \times 10^{-4}Nf - 0.137Nd - 1.25fd \quad (7)$$

$$El = -12.6 + 0.091N - 0.093f + 64.03d - 4.63N^2 - 1.06f^2 - 125.1d^2 - 8 \times 10^{-5}Nf + 5.37 \times 10^{-3}Nd + 0.53fd \quad (8)$$

where N is the tool rotary speed, f is the travel speed, and d is the plunge depth. Also, TS, HV, and EL are tensile strength, hardness, and elongation, respectively.

To check the adequacy and accuracy of the developed mathematical models, ANOVA has been performed, and its results were presented in Tables 7, 8, and 9 for tensile strength, hardness, and elongation, respectively. From the tables, it is seen that the models' F values for TS, HV, and EL are 9.1, 10.6, and 14.73, respectively. The values imply that the model terms are significant. There are only limited chances that the

Table 6 experiments of second stage along with measured values of TS, HV, and EL

No	Process factors			Responses		
	Tool speed (RPM)	Welding speed (mm/min)	Plunge depth (mm)	Tensile strength (MPa)	Hardness (HV)	Elongation (%)
1	600	40	0.1	136	61	25.62
2	1000	40	0.1	145	70	29.45
3	600	80	0.1	156	81	19.66
4	1000	80	0.1	152	75	21.36
5	600	40	0.3	162	85	33.7
6	1000	40	0.3	151	74	37.11
7	600	80	0.3	163	86	31.15
8	1000	80	0.3	155	78	34.13
9	460	60	0.2	163	87	19.66
10	1140	60	0.2	140	64	34.13
11	800	24	0.2	162	86	39.66
12	800	97	0.2	153	77	22.21
13	800	60	0.03	171	95	20.09
14	800	60	0.37	165	89	37.11
15	800	60	0.2	178	103	32.43
16	800	60	0.2	192	117	32.43
17	800	60	0.2	189	114	32
18	800	60	0.2	190	115	32.56
19	800	60	0.2	188	117	32.5
20	800	60	0.2	194	116	32.45

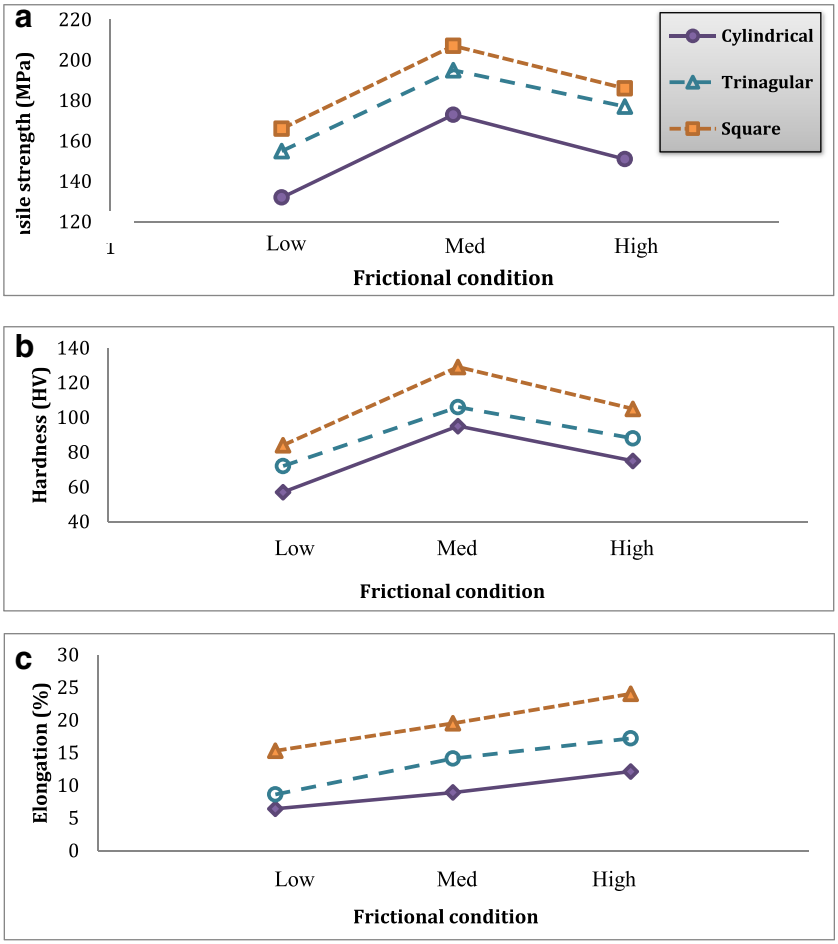

Fig. 3 Effects of tool pin profile on **a** tensile strength, **b** hardness, and **c** elongation

models' "*F* value" could occur due to noise. Values of Prob > F less than 0.05 indicate that the model terms are significant. Therefore, terms such as *N*, *f*, *d*, *Nf*, *Nd*, and *df* are insignificant for tensile strength and hardness. Also, terms such as f^2, *Nf*, *Nd*, and *df* do not have a significant effect in the construction of the regression model of elongation. In addition, the "Lack-of-fit *F* values" of 3.22, 3.22, and 2.11 for TS, HV, and EL indicate that the lack of fit for developed models is not

Table 7 The ANOVA results for modeling tensile strength by RSM

Source	Sum of Square	Degree of freedom	Mean of square	*F* value	Prob > F
model	5429.98	9	603.33	9.1	0.0009
N	203.22	1	203.22	3.2	0.1088
f	20.82	1	20.82	0.31	0.5558
d	74.56	1	74.56	1.14	0.3114
N^2	2855.16	1	2855.16	43.54	<0.0001
f^2	2059.41	1	2059.41	31.4	0.0002
d^2	978.94	1	978.94	14.93	0.0031
Nf	12.5	1	12.5	0.19	0.6717
Nd	72	1	72	1.1	0.3194
fd	60.5	1	60.5	0.92	0.3594
Residual	655.77	10	65.57	–	–
Lack of fit	500.27	5	100.05	3.22	0.1128
Pure error	155.5	5	31.1		–

R^2 0.8922, R^2_{Adjusted} 0.7958

Table 8 The ANOVA results for modeling hardness by RSM

Source	Sum of squares	Degree of freedom	Mean of squares	*F* value	Prob > F
Model	5777.58	9	641.95	10.6	0.0005
N	218.94	1	218.94	3.62	0.0864
f	16.18	1	16.18	0.27	0.6164
d	49.15	1	49.15	0.81	0.3887
N^2	3040.77	1	3040.77	50.23	<0.0001
f^2	2217.49	1	2217.49	36.63	0.0001
d^2	1088.83	1	1088.83	17.98	0.0017
Nf	18	1	18	0.3	0.5975
Nd	60.5	1	60.5	1.0	0.3411
fd	50	1	50	0.83	0.3848
Residual	605.42	10	60.5	–	–
Lack of fit	462.09	5	92.42	3.22	0.1124
Pure error	143.3	5	31.1		–

R^2 0.9051, R^2_{Adjusted} 0.8902

significant. The R^2 values of the model are near to 1; this indicates that the models can be used to navigate the design space.

3.3 Optimization and confirmation

There are many statistical techniques for solving multiple response problems like overlaying the contour plot for each response, constrained optimization problems, and desirability approach. The desirability method is recommended due to its simplicity and availability in the software, and it provides flexibility in weighing and giving importance for individual response. Solving such multiple-response optimization problems using this technique is involved for combining multiple responses into a dimensionless measure of performance called the *overall desirability function* [28].

In the present work, the individual desirability of each response, d_i, was calculated using Eqs. 9, 10, and 11. In order to perform optimization by desirability approach, the process responses with different desirability should be singularized in a unique function. Hence, it is necessary that the responses are firstly normalized to construct a unique desirability function [29]. Depending on whether a particular response *di* is to be maximized or minimized, a different desirability function can be used. For the goal of higher the better, Eq. 4 is used to normalize the responses with desirability of maximum. On the other hand,

Table 9 The ANOVA results for modeling elongation by RSM

Source	Sum of squares	Degree of freedom	Mean of square	*F* value	Prob > F
Model	692.51	9	76.95	14.73	0.0001
N	96.25	1	96.25	18.42	0.0016
f	175.29	1	175.29	0.27	0.0002
d	344.83	1	344.83	33.55	<0.0001
N^2	49.37	1	49.37	66.01	0.0118
f^2	2.57	1	2.57	9.45	0.4987
d^2	22.45	1	22.45	0.49	0.0649
Nf	0.82	1	0.82	4.3	0.7004
Nd	0.092	1	0.092	0.16	0.8968
fd	9.07	1	9.07	0.018	0.2169
Residual	52.24	10	5.22	–	–
Lack of fit	52.05	5	10.41	2.11	0.3345
Pure error	0.19	5	0.038		–

R^2 0.9299, R^2_{Adjusted} 0.8667

Table 10 Optimization criterion

Factors/responses	Criterion	Importance
Tool rotary speed (RPM)	In range of 600–1000	–
Welding speed (mm/min)	In range of 0.1–0.3	–
Plunge depth (mm)	In range of 0.03–0.37	–
Tensile strength (MPa)	Maximize	*** (3)
Hardness (V)	Maximize	*** (3)
Elongation (%)	Maximize	*** (3)

for the goal of lower the better, Eq. 10 is used to normalize the responses with desirability of minimum. Because in the present study all the three responses should be maximized, Eq. 4 is used for normalization.

The shape of the desirability function can be changed for each goal by the weight field "w_i." Weights are used to give more emphasis to the upper/lower bounds or to emphasize the target value. Weights could be ranged between 0.1 and 10; a weight greater than 1 gives more emphasis to the goal, while weights less than 1 give less emphasis. When the weight value is equal to 1, this will make the d_is vary from 0 to 1 in a linear mode. In the desirability objective function (D), each response can be assigned an importance (r), relative to the other responses. Importance varies from the least important value of 1 and the most important value of 5. If the varying degrees of importance are assigned to the different responses, the overall objective function is shown in Eq. (6) below, where n is the number of responses in the measure and r_i is the target value of the ith response [3, 15].

For goal of maximum, the desirability will be defined by

$$d_i = \begin{cases} 0 & Y_i < Low_i \\ \left(\dfrac{Y_i - Low_i}{High_i - Low_i}\right)^w & Low_i < Y_i < High_i \\ 1 & Y_i > High \end{cases} \quad (9)$$

For goal of minimum, the desirability will be defined by

$$d_i = \begin{cases} 1 & Y_i < Low_i \\ \left(\dfrac{Y_i - Low_i}{High_i - Low_i}\right)^w & Low_i < Y_i < High_i \\ 0 & Y_i > High \end{cases} \quad (10)$$

$$D = \left(\prod_{i=1}^{n} d_i^{r_i}\right)^{1/\sum r_i} \quad (11)$$

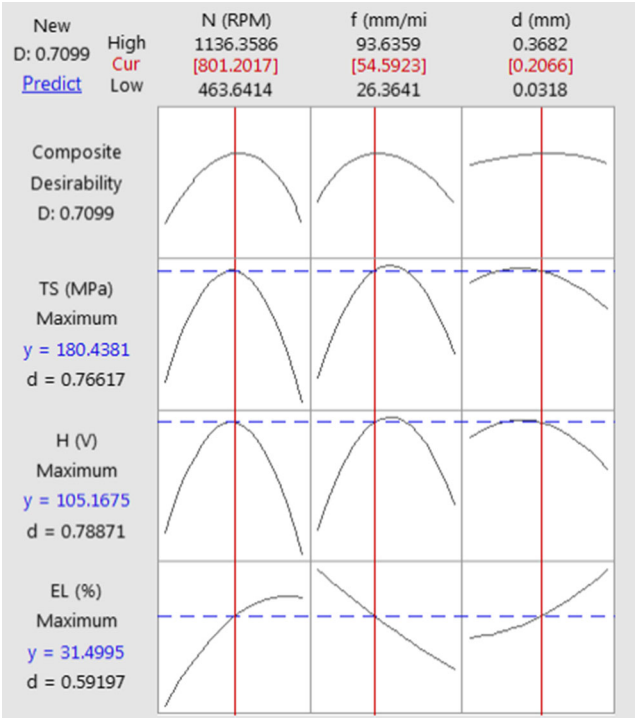

Fig. 4 Exhibition of optimal results based on numerical optimization obtained by MINITAB

According to this technique, the desirable function can find one point or more for numerical optimization of the process.

The desirability function would satisfy all responses with high or low limit of requirements and search for optimum experimental condition for welding performance. The ultimate goal is to produce the maximum TS, HV, and EL, simultaneously. To determine the optimal experiment condition, Design-Expert and MINITAB 16 statistical software package are utilized. Here, Design-Expert is used for numerical and graphical optimization and MINITAB graphs are used to corroborate the obtained results.

To perform multicharacteristic optimization by desirability approach, firstly the optimization criteria should be identified. Table 10 presents the defined criterion for optimization. In contrast, Table 11 presents the optimal solutions based on the identified criterion. Also, Fig. 4 corroborates the obtained numerical optimal solutions which were obtained through the MINITAB software.

In order to verify the optimal results, a confirmatory experiment has been carried out taking into account the parameter setting of Table 11 as a process factor. After

Table 11 Optimal results as obtained by Design-Expert based on identified criterion

N (RPM)	f (mm/min)	d (mm)	TS (MPa)	H (V)	EL (%)	Desirability (%)
797.13	56	0.25	187.35	112.17	35.1523	0.806

Table 12 Comparison between results of confirmatory experiment and those derived from optimization approach (*N* 800 *RPM*, *f* 60 *mm/min*, and *d* 0.25)

Response	Optimization approach	Confirmatory experiment	Error (%)
TS (MPa)	187.35	174	7.6
H (V)	112.1	106	5.7
EL (%)	35.1	33	6.3

performing the experiment, results of the confirmatory experiment were compared with those obtained through optimization approach. It was found from Table 12 that the optimal solution obtained through the proposed methodology is in good agreement with that derived from the confirmatory experiment. The overall value of error in each response was below than 8 % which implies applicability of the proposed methodology.

4 Discussion

From the results of the previous section, the optimal parameter setting was 800 RPM tool rotary speed, 60 mm/min travel speed, and 0.25 mm plunge depth. In addition, the tool with square pin profile causes maximum quality characteristics. However, the results should be discussed based on friction stir welding process physics. The discussion about the results is presented as follows.

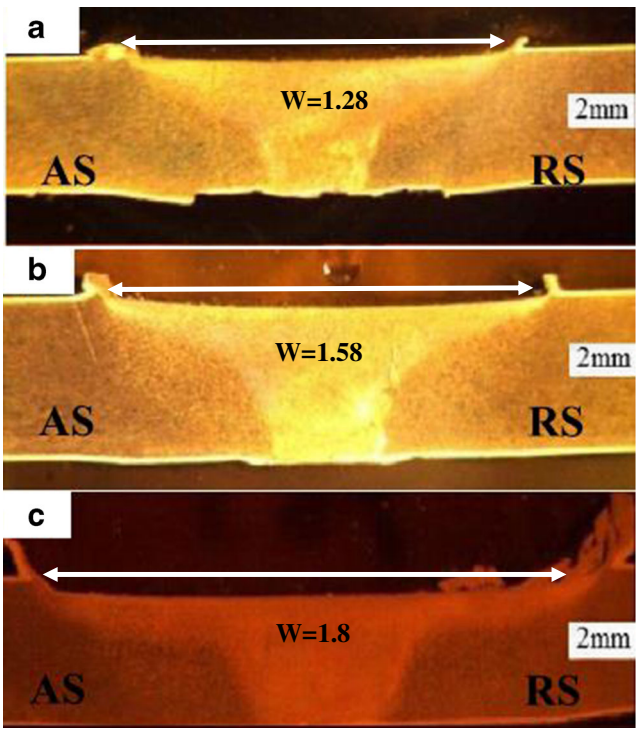

Fig. 5 Weld crown width fabricated by different pin profiles: **a** cylindrical, **b** triangular, and **c** square

4.1 Effect of tool pin profile

As shown in Fig. 3, it is seen that irrespective to frictional condition, tensile strength, hardness, and elongation significantly were affected by the tool pin profile. It is observed that joints fabricated by the square pin profile resulted to have the highest values of mechanical properties. Next to the square pin profile, the straight cylindrical profiles resulted to have desirable properties.

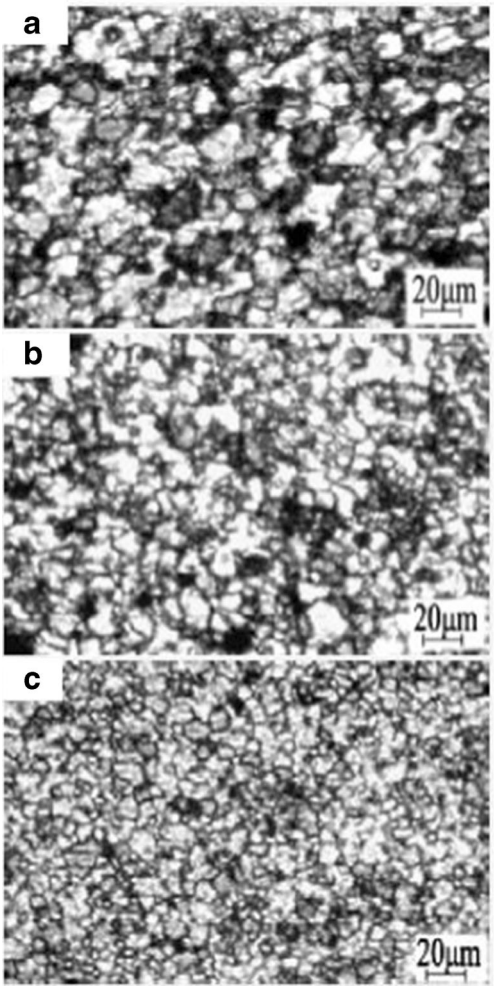

Fig. 6 Microstructure of weld nugget processed by different pin profiles: **a** cylindrical and average diameter is 48.9 μm; **b** triangular and average diameter is 40.6 μm; and **c** square and average diameter is 21.1 μm

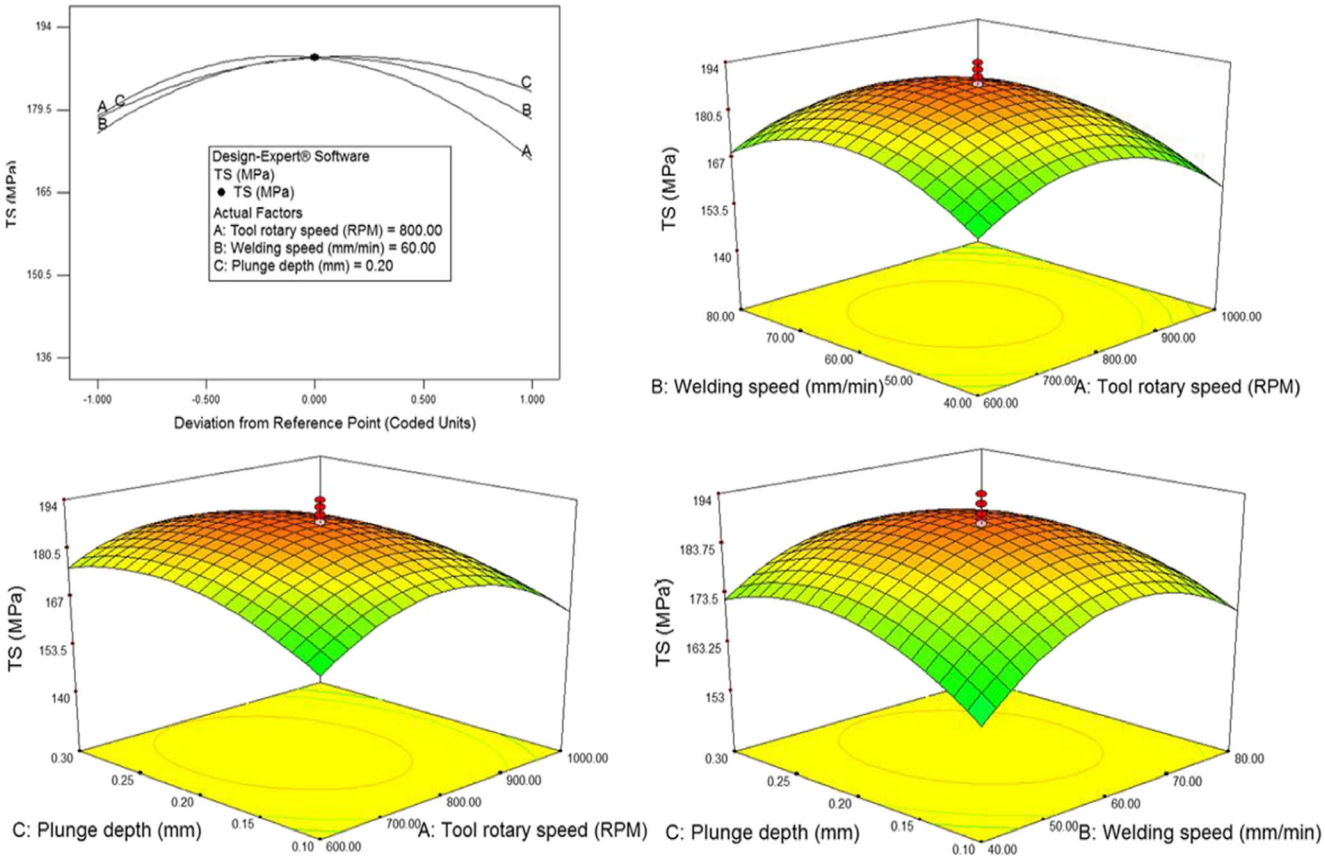

Fig. 7 Perturbation and 3D surface plots showing effects of all the factors on tensile strength

In friction stir welding process, the tool pin will decide the material flow behavior. It plays a crucial role in material flow and in turn regulates the welding speed of the FSW process. Friction stir welds are characterized by well-defined weld nugget and flow contours almost spherical in shape; these contours are dependent on the tool design and welding parameters and process conditions used. The role of tool pin is to shear the material to its back side during translation of the tool, and the inserted rotating pin brings the material at both sides of the joint line to the plastic state, aided by frictional heat input of the shoulder [2].

The tools with square and triangular profiles produce a pulsating stirring action in material flow [30]. The square pin profile leads to better material flow and turbulences. It can improve the stir efficiency due to its four-edged shape. Hence, the mechanical properties induced by this profile are superior rather than the others. Macrostructural observations which are shown in Fig. 5 demonstrate that the square and triangular pin profiles cause wider weld nugget formation due to better material flow that causes higher TS and EL. On the other hand, microstructural observations of Fig. 6 show that the finer grain distributions are obtained by the use of square and triangular pin profiles that cause higher hardness values. From Fig. 5, it is also found that joints that are fabricated with the square pin profile have wider weld nugget and finer grain distribution

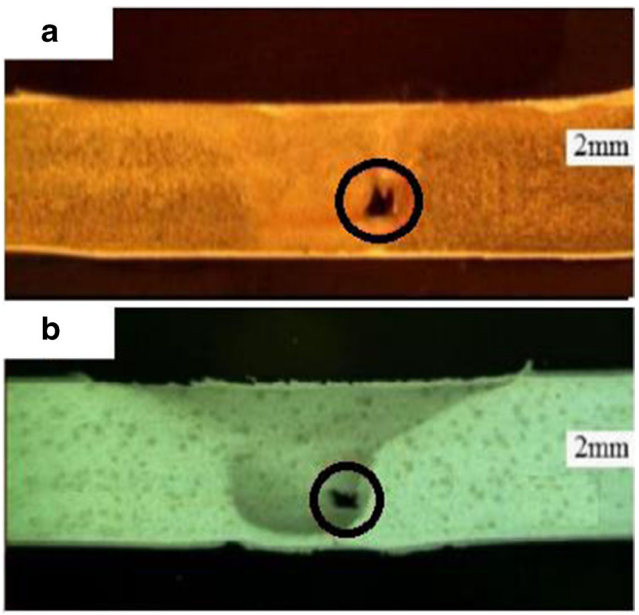

Fig. 8 Defects that formed in the FSP region at various tool rotary speed: **a** 600 RPM and **b** 1000 RPM

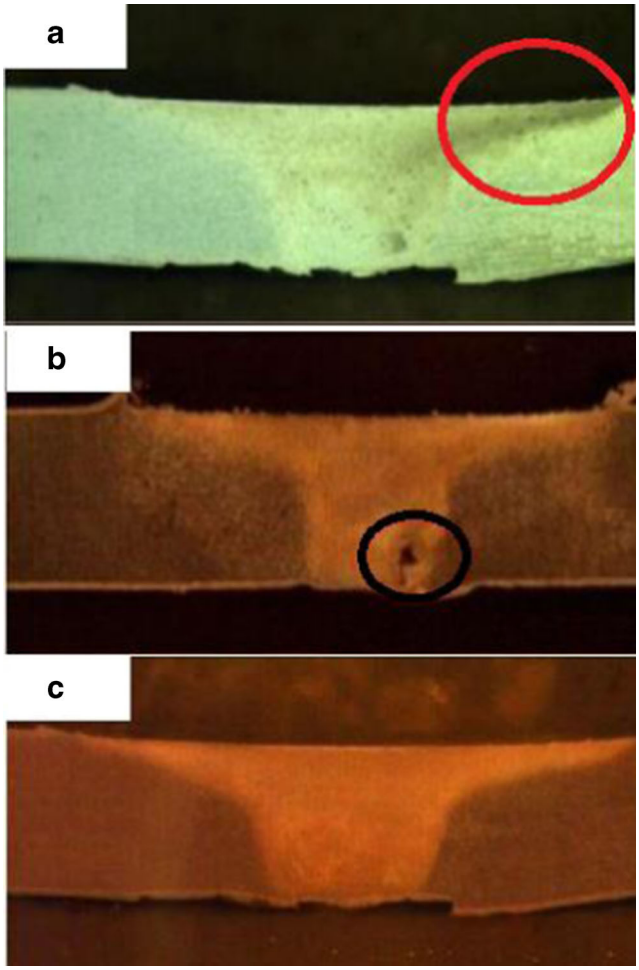

Fig. 9 Macrostructure of FSP region at various welding speeds: **a** kissing bond defect at 40 mm/min; **b** tunnel and narrow weld line in 80 mm/min; **c** defect free at 60 mm/min

while compared to the triangular pin profile. Therefore, it has higher mechanical properties than triangular and cylindrical pin profiles.

4.2 Analyzing tensile strength

In order to analyze the parametric influence of factors on tensile strength, the developed mathematical model of TS (i.e., Eq. 6) is used to plot the graphs. Figure 7 indicates perturbation and 3D surface plots showing effects of process factors on tensile strength of fabricated joints. It is seen that by increasing process factors (i.e., tool rotary speed, welding speed, and plunge depth), the tensile strength increases correspondingly and reaches to a maximum value at intermediate level. Then, by further increase in process factors, the tensile strength decreases.

In the FSW process, the tensile properties and fracture locations of the joints are, to a large extent, dependent on the rotational speed and other parameters. When the joints are associated with defects like pinhole, tunnel, and cracks in the FSP region, the joints failed at the defective area, and if the joints are defect free, the failure locations shifted to the lowest hardness zone. At lower rotational speeds (600 RPM), the welded zone contains defects like tunnel due to insufficient heat input. Thus, the tensile properties (i.e., TS and EL) are relatively low. Also, joints fabricated at higher speeds (i.e., 1000 RPM) contain pin hole defect due to excessive heat input; hence, the tensile strength decreases. Figure 8 demonstrates weld macrostructure that is formed at 600 and 1000 RPM; it is inferred from the figure that defects like tunnel occurred in the FSP region due to insufficient heat input and irregular material flow (Fig. 8a) and defects like pin hole is formed in the FSP region due to excessive heat input (Fig. 8b).

In FSW, the welding speed has a strong impact on productivity in streamlined production of friction stir welding of aluminum alloy sections. A significant increase in welding speed is achieved with high weld quality and excellent joint properties. The softened area is narrower for the higher welding speed than that for the lower welding speed. Thus, the tensile strength of the welded aluminum alloy has a proportional relationship with welding speed [4]. Higher welding speeds are associated with low heat inputs, which result in faster cooling rates of the welded joint. This can significantly reduce the extent of metallurgical transformations taking place during welding (such as solubilization, re-precipitation, and coarsening of precipitates) and, hence, the local strength of individual regions across the weld zone [18].

According to Fig. 7, at a welding speed lower than 60 mm/min (i.e., 40 mm/min), defects such as kissing bond are associated with the FSP zone in the retreating side (Fig. 9a) due to high heat input. On the other hand, when the welding speed goes beyond 60 mm/min (i.e., 80 mm/min and higher), the weld line becomes narrower and some defects such as tunnel are observed at the welded region (Fig. 9b). However, in welding speed of 60 mm/min, the defect-free FSP region is formed which yields high tensile strength.

The plunge depth of the tool shoulder on sheets is in a direct relation with welding axial force. It means that the higher the plunge depth, the higher the axial force and converse. From Fig. 8, when the plunge depth is low (lower than 0.2 mm), the axial force is relatively low and some defects such as crack and pinhole are observed in the welded region due to insufficient heat input. On the other hand, by increasing the plunge depth above 0.2 mm/min, the tensile strength decreases accordingly. When the plunge depth goes beyond a critical value, due to high welding axial force, the thickness of the weld nugget becomes thinner, and it reduces tensile strength.

4.3 Analysis of hardness

In order to analyze the parametric influence of factors on hardness, the developed mathematical model of H (i.e.,

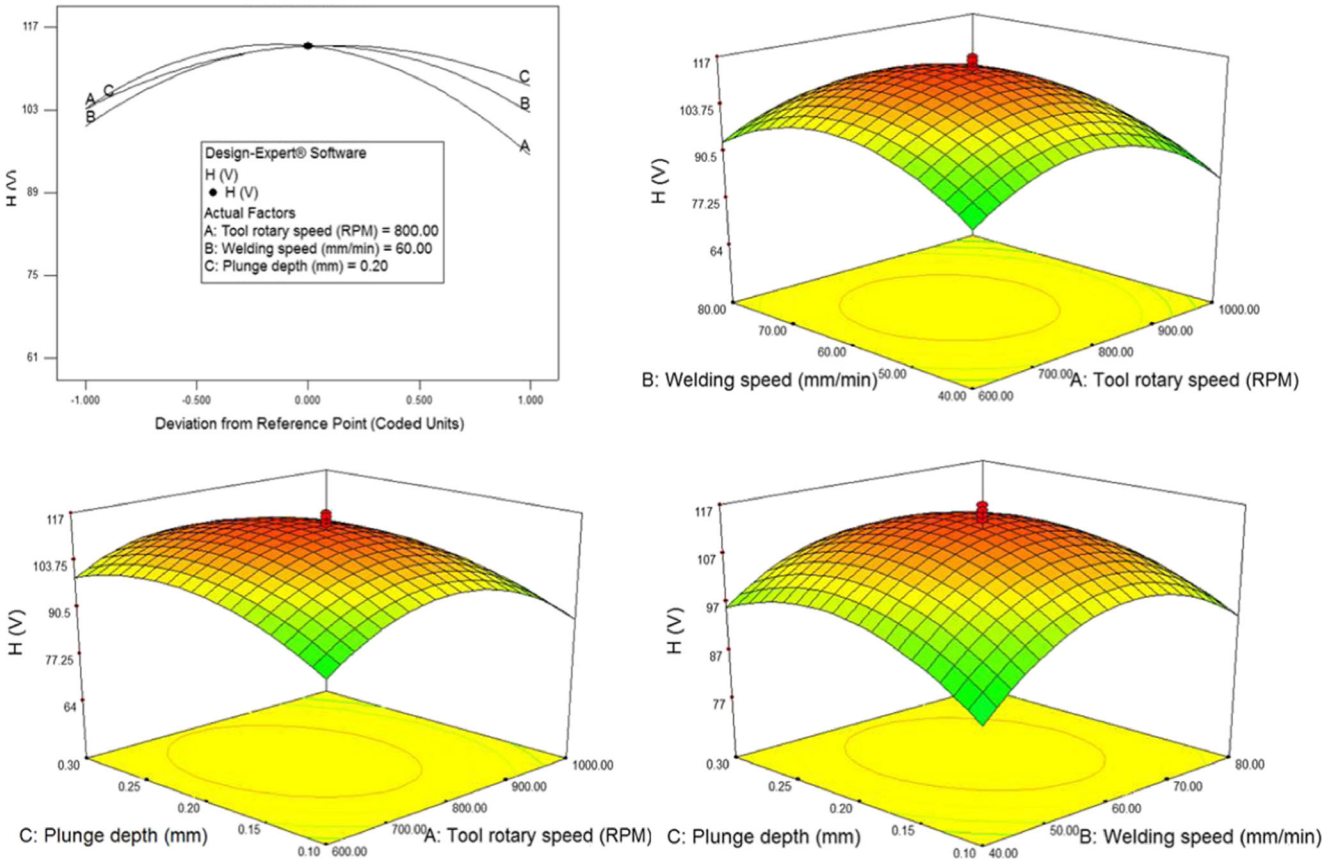

Fig. 10 Perturbation and interaction plots showing effects of processing factors on hardness

Eq. 7) is used to plot the graphs. Figure 10 demonstrates perturbation and 3D surface plots showing effects of process factors on hardness of welded nugget. It is seen from the figure that by increasing process factors (i.e., tool rotary speed, welding speed, and plunge depth), the hardness of the welded zone increases and reaches to a maximum value at their intermediate level. Then, by a further increase in process factors, the hardness decreases.

In friction stir welding, there are two factors that cause the variation of hardness: (i) the size of grains in the welded region and (ii) the formation of intermetallic compositions. These two items are related to heat input and mechanical workings [3].

When the rotary speed is relatively low (lower than 800 RPM), the insufficient heat input prevents formation of intermetallic compositions and causes low hardness. By increasing the tool rotary speed, the sufficient heat input provides appropriate conditions for formation of intermetallic components and yields appropriate hardness. On the other hand, when the rotary speed goes beyond 800 RPM, due to excessive heat input, the grain coarsening causes a decrease in weld nugget hardness. To justify the above claims, an XRD analysis of the joints has been performed. Figure 11 presents XRD spectra of the joint that were obtained. It is seen from the figure that at a high heat input weld, intermetallic compound and strengthening phases like $MgZn_2$ and AlCuMg are intensified that cause higher hardness of the weld nugget.

When the welding speed is relatively low (lower than 60 mm/min), the hardness of the welded region is relatively low. This is due to excessive heat input that causes coarser grain and lower hardness. On the other hand, when the welding speed goes beyond 60 mm/min (i.e.,

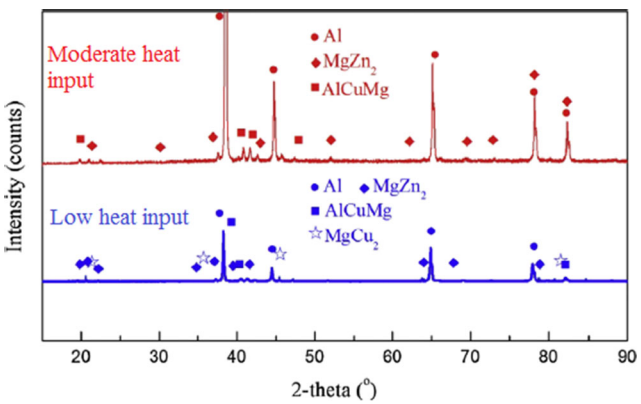

Fig. 11 XRD analysis of weld nugget for **a** advancing side and **b** retreating side

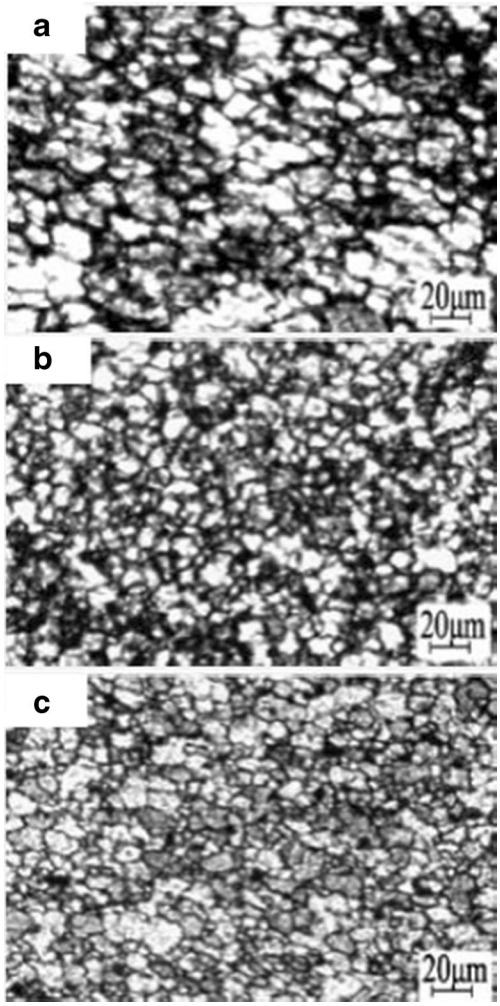

Fig. 12 Microstructure of the weld nugget at different welding speeds: **a** 40 mm/min and average diameter is 38.9 μm; **b** 60 mm/min and average diameter is 29.5 μm; and **c** 80 mm/min and average diameter is 20.7 μm

80 mm/min and higher), the insufficient heat input prevents probability of formation of intermetallic components and hardness decreases. Figure 12 presents microstructure distribution according to different welding speeds. It is seen that when welding travel speed is low, the grain distribution is coarsened which causes low hardness. On the other hand, when the welding travel speed is low, the grain distribution is fine which causes high hardness.

Effect of plunge depth on hardness can be discussed by heat generation. According to the contact model developed by Zhang et al. [16, 17], the mechanical working and corresponding heat generation increase firstly by an increase in tool rotary speed and then by pressure caused by plunge depth. Therefore, the higher value of plunge depth causes higher heat input in weld nugget. In such condition, the size of grains in the welded region increases and causes reduction in hardness.

4.4 Analysis of elongation

The developed RSM model of Eq. 8 is used here to plot the graphs for analyzing elongation. Figure 13 indicates effects of perturbation and 3D surface plots of FSW process factors on elongation. It is seen that an increase in tool rotary speed and axial force results in higher elongation and increase in welding speed leads to decrease in elongation.

The elongation relates to plastic deformation of welded samples in tensile test. Plastic deformation is in a tight direct relation with grain sizes. It means that dynamic recrystallization and grain growth during the welding process lead to better plastic deformation and opposite.

From Fig. 13, it is seen that an increase in tool rotary speed and plunge depth results higher elongation. When the rotary speed of tool and plunge depth increase, the friction between tool shoulder and sheets increases accordingly. Therefore, dynamic recrystallization occurs in the FSP region which causes better plastic deformation and improves elongation [4].

By increasing the welding speed, the cooling rate increases, and due to low heat input condition, dynamic recrystallization and corresponding grain growth are prevented. Hence, the size of grains in the welded region is relatively small, and it reduces plastic formability. Hence, the elongation decreases while increasing welding speed.

5 Conclusion

In the present study, effects of friction stir welding process factors such as tool pin profile, tool rotary speed, welding speed, and plunging depth on mechanical properties such as tensile strength, hardness, and elongation were examined while friction stir welding AA6061 and AA5010 aluminum alloys. Here, experiments were divided to two main stages. At first stage, the aim is to find an appropriate tool pin profile for maximal mechanical properties. After selection of the best tool, it was selected for conducting experiments at the second stage. The aim of the second stage of experiments is to study the effects of rotary speed, welding speed, and plunging depth on the mentioned mechanical properties using RSM. The disability approach was used to find the optimal FSW parameter setting regarding desirable performance. The obtained results can be summarized as follows:

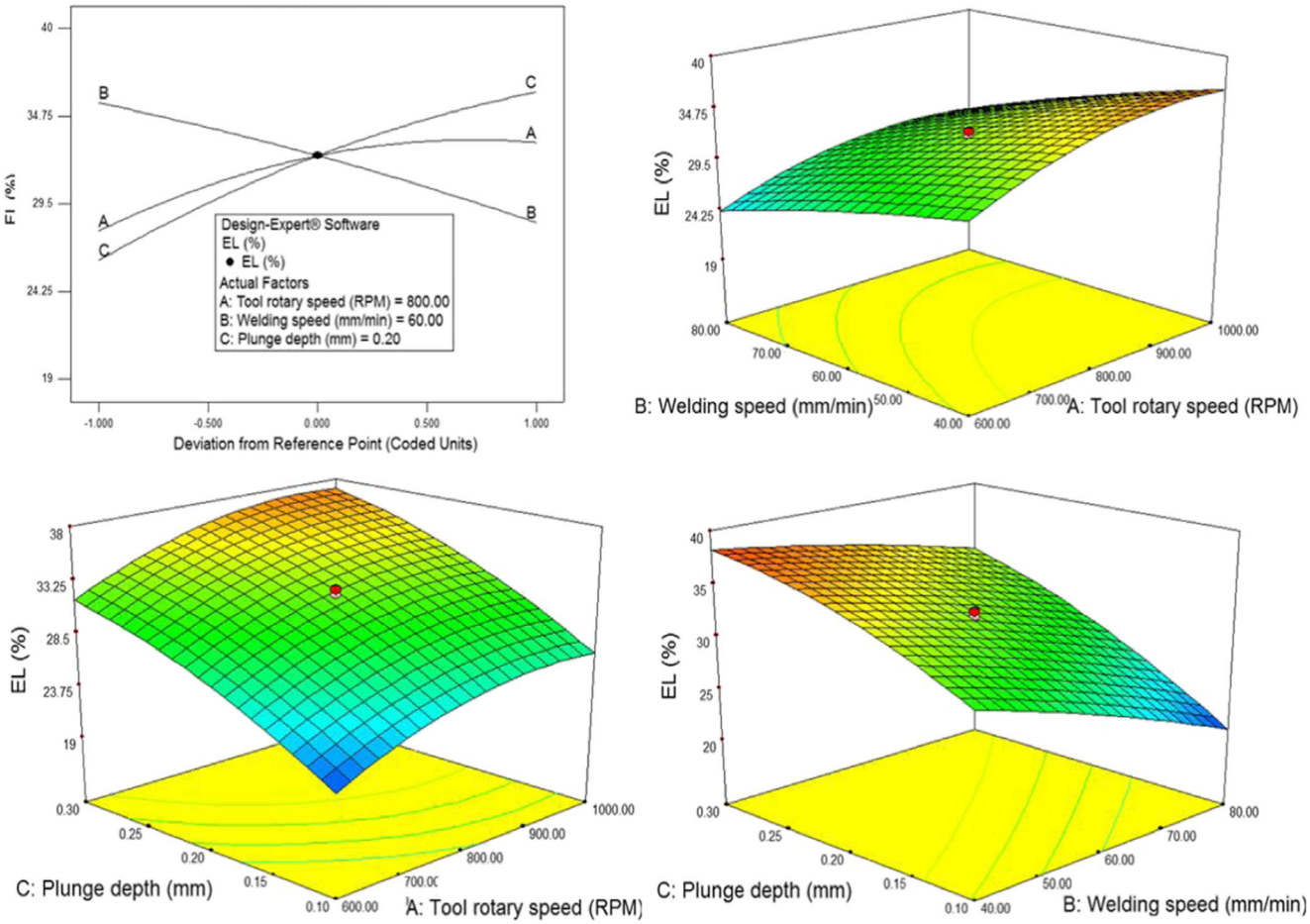

Fig. 13 Perturbation and interaction plots showing effects of processing factors on hardness

1. It was obtained from the results that square type pin profile causes about 22 % improvement in tensile strength, 41 % improvement in hardness, and 100 % improvement in elongation when compared to cylindrical pin profile. The obtained result was in line with the results of Elangovan et al. [3].
2. In construction of mathematical models by RSM, from the analysis of variances, it was found that terms such as *N*, *f*, *d*, *Nf*, *Nd*, and *df* are insignificant for tensile strength and hardness. In addition, terms such as f^2, *Nf*, *Nd*, and *df* do not have a significant effect in construction of regression model of elongation.
3. It was obtained from the parametric analysis of tensile strength and hardness that tool rotary speed of 800 RPM, travel speed of 60 mm/min, and plunge depth of 0.2 mm cause maximum values of TS and H.
4. Parametric analysis showed that to achieve the highest elongation, parameter setting of 1000 RPM, tool rotary speed of 40 mm/min, and travel speed of 0.3 mm plunge depth should be selected.
5. By simultaneous optimization of mechanical properties by desirability function and use of numerical approach, it was obtained that tool rotary speed about 800 RPM, welding speed about 60 mm/min, and plunge depth about 0.25 mm/min are the optimal solution which cause 174 MPa tensile strength, 106 V hardness, and 33 % elongation.
6. The values of tensile strength, hardness, and elongation at optimum level is 67, 130, and 78 % of AA5010 parent material that show desirable welding quality characteristics.
7. The obtained optimal results were verified through confirmatory experiment, and the findings showed that the proposed approach can predict the optimal solutions with overall error values lower than 8 %.
8. It was found that at optimal condition, defect-free weld line and fine grain structure (i.e., with average diameter between 20 to 30 μm) with considerable amount of intermetallic compound like AlCuMg are formed which cause improvement in mechanical properties. The results were in agreement with research from Rajakumar et al. [2].

References

1. Koilraj M, Sundareswaran V, Vijayan S, Rao SK (2012) Friction stir welding of dissimilar aluminum alloys AA2219 to AA5083—optimization of process parameters using Taguchi technique. Mater Des 42:1–7
2. Elangovan K, Balasubramanian V (2008) Influences of tool pin profile and axial force on the formation of friction stir processing zone in AA6061 aluminium alloy. Int J Adv Manuf Technol 38: 285–295
3. Elangovan K, Balasubramanian V, Babu S (2009) Predicting tensile strength of friction stir welded AA6061 aluminum alloy joints. Mater Des 30:188–193
4. Lee WB, Yeon YM, Jung SB (2004) Mechanical properties related to micro structural variation of 6061 Al alloy joints by friction stir welding. Mater Trans 45(5):1700–1705
5. Ramalu PJ, Narayanan RG, Kailas SV, Reddy J (2013) Internal defect and process parameter analysis during frictio n stir welding of Al 6061 sheets. Int J Adv Manuf Technol 65:1515–1528
6. Yong-Jai KWON, Seong-Beom S, Dong-Hwan PARK (2009) Friction stir welding of 5052 aluminum alloy plates. Trans Nonferrous Metals Soc China 19:s23–s27
7. Min-Su HAN, Seung-Jun LEE, Jae-Cheul PARK, Seok-Cheol KO, Yong-Bin WOO, Seong-Jong KIM (2009) Optimum condition by mechanical characteristic evaluation in friction stir welding for 5083-O Al alloy. Trans Nonferrous Metals Soc China 19:s17–s22
8. Moshwan R, Yusof F, Hassan MA, Rahmat SM (2015) Effect of tool rotational speed on force generation, microstructure and mechanical properties of friction stir welded Al–Mg–Cr–Mn (AA 5052-O) alloy. Mater Des 66:118–128
9. Aval HJ, Serajzadeh S, Kokabi AH (2011) Thermo-mechanical and microstructural issues in dissimilar friction stir welding of AA5086–AA6061. J Mater Sci 46(10):3258–3268
10. Alvarez P, Arruti E, Aldanondo E, Alberto E (2012) Understanding material flow in FSW and its implications. Proceedings of the second international conference FSWP'2012, ISBN: 978-2- 911256-72-1, France
11. Palanivel R, Mathews PK, Murugan N, Dinaharan I (2012) Effect of tool rotational speed and pin profile on microstructure and tensile strength of dissimilar friction stir welded AA5083-H111 and AA6351-T6 aluminum alloys. Mater Des 40:7–16
12. Leitao C, Louro R, Rodrigues DM (2012) Analysis of high temperature plastic behavior and its relation with weldability in friction stir welding for aluminum alloys AA5083–H111 and AA6082–T6. Mater Des 37:402–409
13. Kasman Ş (2013) Multi-response optimization using the Taguchi-based grey relational analysis: a case study for dissimilar friction stir butt welding of AA6082-T6/AA5754-H111. Int J Adv Manuf Technol 68(1–4):795–804
14. Zhang Z (2008) Comparison of two contact models in the simulation of friction stir welding process. J Mater Sci 43(17):5867–5877
15. Zhang Z, Chen TJ (2012) Computational investigations on reliable finite element-based thermomechanical-coupled simulations of friction stir welding. Int J Adv Manuf Technol 60:959–975
16. Zhang Z, Zhang HW (2014) Solid mechanics-based Eulerian model of friction stir welding. Int J Adv Manuf Technol 72:1647–1653
17. Zhang Z, Chen TJ, Zhang ZW, Zhang HW (2011) Coupled thermo-mechanical model based comparison of friction stir welding processes of AA2024-T3 in different thicknesses. J Mater Sci 46: 5815–5821
18. Zhang Z, Wu Q, Gruijicic M, Wan ZY (2015) Monte Carlo simulation of grain growth and welding zones in friction stir welding of AA6082-T6. J Mater Sci. doi:10.1007/s10853-015-9495-x
19. Zhang Z, Wu Q, Zhang HW (2015) Prediction of fatigue life of welding tool in friction stir welding of AA6061-T6. Int J Adv Manuf Technol. doi:10.1007/s00170-016-8475-x
20. Aval HJ, Serajzadeh S, Kokabi AH (2012) Experimental and theoretical evaluations of thermal histories and residual stresses in dissimilar friction stir welding of AA5086-AA6061. Int J Adv Manuf Technol 61:149–160
21. Al-Badour MN, Shuaib A, Bazoune A (2014) Thermo-mechanical finite element model of friction stir welding of dissimilar alloys. Int J Adv Manuf Technol 72:607–617
22. Kishore VR, Arun J, Padmanabhan R, Balbasubramanian V (2015) Parametric studies of dissimilar friction stir welding using computational fluid dynamics simulation. Int J Adv Manuf Technol 80: 91–98
23. Padmanaban R, Balusamy V, Saikirishna V, Gopath NK (2014) Simulated annealing based parameter optimization of friction stir welding of dissimilar aluminum alloy. Procedia Engineering 97: 864–870
24. Elatharasna G, Senthil Kumar VS (2012) Modeling and oprimiation of friction stir welding parameters for dissimilar aluminum alloys using RSM. Procedia Engineering 38:3477–3481
25. Gupta SK, Pandey KN, Kumar R (2016) Multi-objective optimization of friction stir welding process parameters for joining of dissimilar AA5083/AA6063 aluminum alloys using hybrid approach. Proceedings of the Institution of Mechanical Engineers, Part L: Journal of Materials Design and Applications, 1464420715627294
26. Palanivel R, Mathews PK, Murugan N (2013) Optimization of process parameters to maximize ultimate tensile strength of friction stir welded dissimilar aluminum alloys using response surface methodology. J Cent South Univ 20(11):2929–2938
27. Arora A, Nadan R, Reynolds AP, Debroy T (2009) Torque, power requirement and stir zone geometry in friction stir welding through modeling and experiments. Scr Mater 60:13–16
28. Shayan AV, Azar Afza R, Teimouri R (2013) Parametric study along with selction of optimal solutions in dry wire cut machining of cemented tungsten carbide (WC-Co). J Manuf Process 15(4): 644–658
29. Babajanzade-Roshan S, Behboodi-Jooibari M, Teimouri R, Asgharzade-Ahmadi G, Falahati-Naghibi M, Sohrabpoor H (2013) Optimization of friction stir welding process of AA7075 aluminum alloy to achieve desirable mechanical properties using ANFIS models and simulated annealing algorithm. Int J Adv Manuf Technol 69(5):1803–1818
30. Elangovan K, Balasubramanian V (2007) Influences of pin profile and rotational speed of the tool on the formation of friction stir processing zone in AA2219 aluminium alloy. Mater Sci Eng A 459(1):7–18